

# A static quantum embedding scheme based on coupled cluster theory

Avijit Shee,<sup>1</sup> Fabian M. Faulstich,<sup>2</sup> Birgitta Whaley,<sup>1,3</sup> Lin Lin,<sup>4,5</sup> and Martin Head-Gordon<sup>1</sup>

<sup>1</sup>*Department of Chemistry, University of California, Berkeley, USA*

<sup>2</sup>*Department of Mathematics, Rensselaer Polytechnic Institute, Troy, NY 12180, USA*

<sup>3</sup>*Berkeley Center for Quantum Information and Computation, Berkeley*

<sup>4</sup>*Department of Mathematics, University of California, Berkeley, CA 94720, USA*

<sup>5</sup>*Applied Mathematics and Computational Research Division,  
Lawrence Berkeley National Laboratory, Berkeley, CA 94720, USA*

We develop a static quantum embedding scheme, utilizing projection equations to solve coupled cluster (CC) amplitudes. To reduce the computational cost (for example, of a large basis set calculation), we solve the local fragment problem using a high-level coupled cluster method and address the environment problem with a lower-level Møller-Plesset (MP) perturbative method. This embedding approach is consistently formulated within the coupled cluster framework and will be called MP-CC. We demonstrate the effectiveness of our method through several prototypical molecular examples by analyzing a global quantity, that is, the total correlation energy of the system in the study of potential energy curves (PEC) and thermochemical reaction energies. We have shown that our method can achieve comparable accuracy both with a small and large basis set when the fragment Hilbert space size remains the same. Additionally, our results indicate that increasing the fragment size can systematically enhance the accuracy of observables, approaching the precision of the full coupled cluster solver.

## I. INTRODUCTION

Coupled cluster (CC) theory provides the best balance between efficiency and accuracy in the simulation of weak to moderately correlated molecules. However, CC theory with even the simplest truncation, that is, singles and doubles, still has compute costs that scale steeply with problem size, as  $\mathcal{O}(N^6)$ . This precludes a large basis set calculation of molecular systems containing many atoms, without the use of linear scaling methods.<sup>[1–4]</sup> To overcome the bottleneck of large basis set calculations with CC, many methods have been proposed, for example, explicitly correlated R12/F12 methods [5], diagrammatic separation-based extrapolation [6], an empirical function based extrapolation [7] among many others.

In this work, we aim at addressing the large basis set problem from a quantum embedding perspective. In quantum embedding approaches, one first identifies an important – and preferably local – region of the system denoted fragment (F). The remainder of the system is referred to as environment (E) and is treated by a low-scaling method, e.g., HF/DFT or a perturbative method. For the fragment problem, one first evaluates a coupling potential ( $\Delta$ ) between the environment and the fragment. This coupling potential is then incorporated into the fragment Hamiltonian treating the fragment problem as an open-quantum system. The fragment problem is solved with a high-accuracy method, for example, full CI (FCI) [8], Quantum Monte Carlo (QMC) [9] or Density Matrix Renormalization Group (DMRG) [10]. This highly accurate solution on the fragment is subsequently used to self-consistently update  $\Delta$ . In the same spirit, for a large basis set calculation, we will identify a smaller active/fragment orbital space and embed it inside the remainder of the system. The fragment problem will subsequently be described by a renormalized interaction, and

solved by a CC method truncated up to a certain excitation rank. The environment problem in this theory is spanned by the large basis set, and treated by a perturbative method, which can be conveniently treated by a low-order polynomial scaling algorithm [11–13]. The cost of the fragment problem remains constant with the increase of basis set size and thus reduces the overall cost.

Our work is inspired by the recent work of Kowalski and co-workers [14, 15]. This approach constructs a downfolded Hamiltonian for the fragment problem employing a lower excitation rank CC method, when a solution to the fragment problem with higher rank CC is sought. Our proposed method utilizes this concept while creating a more versatile framework with two sets of CC equations: one for the environment and one for the fragment. Furthermore, we invoke a self-consistency condition between the fragment and the environment based on the “global” CC amplitudes. This particular aspect of the theory has also been previously included in the multi-level CC (MLCC) works by Koch and co-workers [16, 17]. However, certain differences with that approach in terms of the general framework and computational implications will be elaborated in Appendix A.

Besides the embedding approaches, we will compare the current method with energy additivity schemes. At a lower level of accuracy, there is a long history of such approximations in quantum chemistry, including the Gaussian- $n$  methods (G1-G4)[18–21], the Weizmann- $n$  methods (W1-W4)[22–24], the HEAT protocol[25], etc. These can be regarded as very simple uncoupled approximations to the embedding problem. As a simple example, the basis set correction to an expensive coupled cluster calculation such as CCSD(T) might be approximated using a far less demanding approach such as second-order Møller-Plesset theory (MP2) that exhibits similar basis

set dependence via:

$$E_{\text{Composite}} \approx E_{\text{CC/small}} + (E_{\text{MP2/large}} - E_{\text{MP2/small}}) \quad (1)$$

Our numerical comparison in Section IV will reveal the regimes where such approximations are not adequate.

The remainder of the manuscript is organized as follows: We will elaborate on the theoretical details of the proposed method in Section II. As is common for embedding methods, it is important to choose a suitable local basis that describes the fragment problem well. Note that the results of embedding methods are in general not invariant with respect to this choice. We describe the choice of basis employed in the simulation presented in this manuscript in Section III. Finally, we will show and analyze a few prototypical numerical examples with the current approach in Section IV.

## II. EMBEDDED COUPLED CLUSTER FORMALISM

Coupled cluster (CC) theory is a wave function approach that expresses the ground-state wave function using an exponential parametrization. Given a single Slater determinant reference state, e.g., the Hartree-Fock (HF) determinant  $|\Phi_0\rangle$ , any intermediately normalized state  $|\Psi\rangle$ , i.e.,  $\langle\Psi|\Phi_0\rangle = 1$ , can be uniquely written as  $e^T|\Phi_0\rangle$ , where the cluster operator

$$T = \sum_{l>0} t_l X_l$$

induces various ranks of hole-particle excitations  $X_l$ , see e.g. [26]. The CC amplitudes, denoted by  $\mathbf{t}$ , are determined through the projective equations:

$$\langle\chi_l|\bar{H}|\Phi_0\rangle = 0 \quad \forall l > 0, \quad (2)$$

where

$$\bar{H} = e^{-T} H e^T \quad (3)$$

and  $\langle\chi_l|$  denotes the excited Slater determinants with an excitation rank  $l > 0$ . The corresponding CC energy is then given by

$$E_{\text{CC}} = \langle\Phi_0|\bar{H}|\Phi_0\rangle. \quad (4)$$

For computational viability, the most commonly employed CC variant is CCSD, where  $T$  comprises excitations up to a maximum of rank two, i.e.,

$$T = \sum_{i,a} t_i^a X_i^a + \frac{1}{4} \sum_{i,j,a,b} t_{ij}^{ab} X_{ij}^{ab}. \quad (5)$$

However, even this approach, scaling  $\sim \mathcal{O}(N^6)$  with number of atomic basis functions in the molecule,  $N$ , becomes computationally demanding when applied to

larger systems (unless local correlation approximations are employed). We here propose and numerically scrutinize an approximation to CCSD that is inspired by quantum embedding theory. The core concept of this variant is well-known: the recognition that certain CC amplitudes in  $t_i^a$  and  $t_{ij}^{ab}$  possess greater physical significance than others, if expressed in a suitable basis (for example, local, natural orbital etc). Our proposed approach aims to identify and accurately approximate these critical amplitudes, while the less significant amplitudes are approximated with reduced precision (vide infra). This strategy is designed to maintain high accuracy while simultaneously reducing the overall computational complexity. We therefore name this approach the many-body perturbation coupled-cluster (MP-CC) method.

Underlying the MP-CC approach is a partition of the total orbital space into two sets: the fragment (F) orbitals and the environment (E) orbitals, where the fragment orbitals describe the chemically more relevant region which we seek to describe with high accuracy. In this article, the fragment orbitals are characterized by intrinsic atomic orbital (IAO)s [27] expressed in a smaller atomic orbital basis than the actual basis set of the calculation. The environment orbitals, on the other hand, will describe the additional virtual orbitals associated with a larger atomic orbital basis, and a few core occupied orbitals that is not contained in the fragment orbital space. As discussed later, other choices are possible such as the fragment orbitals describing just a single local site of particular interest (e.g. a catalytic active site), or a set of local sites.

Once a partition is made, there are three classes of cluster operators:  $T^{\text{F}}$ ,  $T^{\text{E}}$ ,  $T^{\text{M}}$ , where ‘‘M’’ stands for ‘‘mixed’’, i.e., the CC amplitudes that determine  $T^{\text{M}}$  mix fragment and environment orbitals. Subsequently, we will use uppercase letters (I, J, K, L,... for hole type; A, B, C, D,... for particle type) to denote orbitals in the fragment, and lowercase letters (i, j, k, l,... for hole type; a, b, c, d,... for particle type) for orbitals in the environment.

In general, the chosen partition moreover yields

$$n_v = n_{v,\text{inact}} + n_{v,\text{act}} \quad \text{and} \quad n_o = n_{o,\text{inact}} + n_{o,\text{act}}. \quad (6)$$

Here,  $n_v$  and  $n_o$  represent the total counts of virtual and occupied orbitals, respectively. Within these categories,  $n_{\cdot,\text{inact}}$  and  $n_{\cdot,\text{act}}$  denote the numbers of inactive and active orbitals, respectively, hence, the total count of each orbital type is composed of the sum of its inactive and active subsets.

In the spirit of quantum embedding, we will compute the cluster operators  $T^{\text{F}}$ , and  $T^{\text{E}}$  and  $T^{\text{M}}$  using different theoretical frameworks. More precisely, we propose to determine the fragment cluster operator  $T^{\text{F}}$  using the standard CC formalism (the high-level theory), involving a full expansion of  $\bar{H}$  (see Eq. 3) to yield  $\bar{H}_{\text{F,high}}$ . In contrast, the calculation of  $T^{\text{E}}$  and  $T^{\text{M}}$  is based on a lower-order expansion of  $\bar{H}$ , resulting in  $\bar{H}_{\text{E/M,low}}$ . This lower-order expansion offers various options for gaining

a computational advantage, the specifics of which will be elaborated in Sec. II A. Hence, the MP-CC approach results in two (coupled) sets of projective equations:

$$\langle \chi_l^F | \bar{H}_{F,\text{high}} | \Phi_0 \rangle = 0, \quad (7)$$

$$\langle \chi_l^{E/M} | \bar{H}_{E/M,\text{low}} | \Phi_0 \rangle = 0. \quad (8)$$

We emphasize that both  $\bar{H}_{F,\text{high}}$  and  $\bar{H}_{E/M,\text{low}}$  in Eqs. (7) and (8) contain the full set of  $T$ -amplitudes ( $\mathbf{t}^F \cup \mathbf{t}^M \cup \mathbf{t}^E$ ). In other words, although Eq. (7) solves only for  $\mathbf{t}^F$ , the amplitudes  $\mathbf{t}^E$  and  $\mathbf{t}^M$  still enter the equations. Similarly, Eq. (8) solves for  $\mathbf{t}^E$  and  $\mathbf{t}^M$  in the presence of  $\mathbf{t}^F$ . Therefore, Eqs. (7) and (8) should be solved self-consistently. Note that the total CC energy expression remains as Eq. (4).

Combining the energy and projection conditions yields the Lagrangian:

$$\begin{aligned} \mathcal{L}(\mathbf{t}, \lambda) = & \langle \Phi_0 | \bar{H} | \Phi_0 \rangle + \langle \Phi_0 | \Lambda^E \bar{H}_{E,\text{low}} | \Phi_0 \rangle \\ & + \langle \Phi_0 | \Lambda^M \bar{H}_{M,\text{low}} | \Phi_0 \rangle + \langle \Phi_0 | \Lambda^F \bar{H}_{F,\text{high}} | \Phi_0 \rangle. \end{aligned} \quad (9)$$

Here  $\Lambda = \sum_{l>0} \lambda_l X_l^\dagger$  consists of the dual variables  $\lambda_l$ , ensuring that the constraints in Eqs. (7) and (8) are satisfied, and the adjoint of the excitation operator  $X_l$ . The working equations correspond to a first-order optimality condition of the Lagrangian, i.e.,

$$\begin{cases} \frac{\partial \mathcal{L}}{\partial \mathbf{t}} = 0, \\ \frac{\partial \mathcal{L}}{\partial \lambda^\alpha} = 0, \quad \alpha \in \{E, F, M\}. \end{cases} \quad (10)$$

Note that compared to other embedding approaches, the Lagrangian in Eq. (9) enables us to access a broader range of (global) static observables beyond the energy, by employing analytic energy derivative techniques [28, 29].

### A. Environment amplitude equations

We employ two distinct approaches to the lower-order expansion  $\bar{H}_{E/M,\text{low}}$ , both of which are based on perturbative arguments. In the first approach, we use MP2-like projection equations, i.e.,

$$\langle \chi_l^{E/M} | V + [F, T] | \Phi_0 \rangle = 0 \quad (11)$$

to obtain  $T^E$  and  $T^M$ . We emphasize again that  $T$  contains all cluster amplitudes, however, the projective equations (11) are used to determine  $T^E$  and  $T^M$  only. In defining these equations, we have used the partitioned Hamiltonian:  $H = F + V$ , where  $F$  is an unperturbed Hamiltonian or the Fock matrix from HF theory and  $V$  is the two-particle interaction term, expressed in the HF basis. Note that we use normal-ordered operators for  $F$  and  $V$ , though we do not denote it explicitly.

In the second approach, we relax the wave function in the sense of Thouless relaxation [30], while correlation is

treated at the perturbative level. Hence, we make the wave function ansatz

$$|\Psi_\eta\rangle = e^S e^{T_\eta} |\Phi_0\rangle,$$

where  $S$  is a single excitation operator and  $T_\eta$  denotes that any higher-order excitations will be treated at the low-order perturbative level. More precisely, we will assign the perturbative strength  $\eta$  to the interaction term of the Hamiltonian and the resulting projection equations will be truncated in terms of the perturbative order of  $T_\eta$  and  $V$ .

For example, keeping the terms up to first order in perturbation yields the following projective equations for the singles and doubles amplitudes:

$$\langle \chi_s^{E/M} | \tilde{F} + [\tilde{F}, T] | \Phi_0 \rangle = 0 \quad (12)$$

$$\langle \chi_d^{E/M} | \tilde{V} + [\tilde{F}, T] | \Phi_0 \rangle = 0 \quad (13)$$

where  $\tilde{F}$  and  $\tilde{V}$  are up to first-order one- and two-particle operators of the similarity transformed Hamiltonian  $H_\eta$  i.e.,  $\tilde{F}_\eta + \tilde{V}_\eta = e^{-S} H_\eta e^S$ . In the derivation of Eq. (12), and (13) we used the fact that the similarity transformation of  $H_\eta$  with  $e^S$  will not lead to any higher-order perturbative terms, thus the final amplitude equations will be similar to the MP2 amplitude equations, but with the similarity transformed Hamiltonian. Moreover, we note that this transformation will not increase the operator rank of the Hamiltonian.

In Fig. 1, we schematically show the workflow of the proposed method ( $W^F$  is defined in II B). Note that when employing a relaxation of the wave function (i.e., the second approach outlined above) in step 3 (see Fig. 1), the first iteration uses  $S = 0$  implying that Eq. (12) and (13) reduce to Eq. (11). In particular, in the first iteration, the two procedures outlined above yield the same inactive amplitudes. However, in the subsequent iterations, non-zero active singles amplitudes generated from the  $T^F$ -amplitude equations will contribute to Eq. (12) and (13), thus yielding non-zero inactive singles amplitudes.

In contrast to the CC2 equations [31], which address the  $T_1$  amplitude equations to all orders while treating the  $T_2$  amplitude equations only up to the first order, our approach consistently applies a first-order perturbative treatment to both the  $T_1$  and  $T_2$  amplitude equations to determine inactive CC amplitudes. A CC2-like approach has been taken in the Multi-Level CC (MLCC) work by Koch and co-workers to define the inactive CCSD amplitude equations. Similar to the MLCC approach, the computational complexity of the inactive MP-CC amplitude equations is  $\mathcal{O}(n_v^3 n_o^2)$ , at the singles and doubles level. That being said, the inclusion of  $T_3$  amplitudes in the MP-CC framework – where active non-zero  $T_3$

amplitudes induce further relaxation of the environment orbitals – does not increase the complexity of the low-level projection equation. However, with the MLCC approach, the complexity of the low-level projection equations would have been higher, but they approximate the triple excitations only to the active indices to reduce the complexity. For a more detailed discussion on the differences between MLCC and MP-CC, we refer the interested reader to Appendix A. A side-by-side numerical comparison of MLCC and MP-CC is left for future work.

## B. Fragment amplitude equations

An important observation is that in the fragment amplitude equations (7), the Hamiltonian  $\bar{H}_{F,\text{high}}$  is screened by the environment amplitudes  $\mathbf{t}^{E/M}$ . We may rewrite Eq. (7) in the following way:

$$\langle \chi_l^F | e^{-T^F} W_F e^{T^F} | \Phi_0 \rangle = 0, \quad (14)$$

where

$$\begin{aligned} W_F &= [e^{-T^M} e^{-T^E} H e^{T^E} e^{T^M}]_F \\ &= W_{1b,F} + W_{2b,F} + W_{3b,F} + \dots \end{aligned} \quad (15)$$

In Eq. (15), we renormalize the bare Hamiltonian by applying a similarity transformation via  $e^{T^E+T^M}$  and then restrict the orbital indices to the fragment. Note that the similarity transformation increases the rank of  $W_F$  compared to the bare Hamiltonian. However, when solving Eq. (14), we order the operation of the tensors such that we avoid generating higher rank  $W_F$  tensors. This particular construction is conceptually important because it reflects that the low-energy (or for the active region) Hamiltonian is screened by the “high-energy” amplitudes, which is a crucial requirement for the quantum embedding theories [32, 33]. We note that in a similar manner, Kowalski *et. al.* construct a CC downfolded Hamiltonian by using sub-system embedding subalgebras (SES) [15]. In Fig. 1, we schematically show that in step 4 and step 5, we first construct  $W_F$ , and then iteratively solve Eq. (14). The maximum complexity of solving Eq. (14) is  $\mathcal{O}(n_{o,\text{act}}^2 n_{v,\text{act}}^4)$ , thus it scales linearly with the number of fragments. The construction of  $W_F$ , on the other hand, scales as  $\mathcal{O}(n_v^2 n_o^2 n_{o,\text{act}} n_{v,\text{act}})$ , however, this cost is non-iterative.

## III. IMPLEMENTATION

The computational results presented subsequently are obtained using a pilot implementation of the MP-CC method at the singles-doubles truncated level, that is MP-CCSD, based on the Python-based Simulations of Chemistry Framework (PySCF) [34–36]. In this implementation, the amplitude equations are separated into

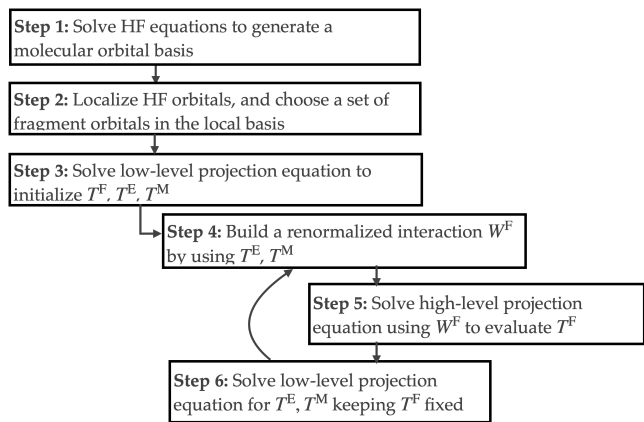


Figure 1. Schematic view of the current embedding scheme.

different classes based on F, E, and M, allowing us to experiment with the different heuristics mentioned in Sec. II A. We conduct all-electron calculations using CCSD as the computational solver in both spin-restricted and spin-unrestricted formulations. For the spin-unrestricted version of MP-CCSD, along with the unrestricted Hartree-Fock (UHF) orbitals, we also allow for restricted open-shell Hartree-Fock (ROHF) orbitals, and the resulting theory will be called the UMP-CCSD and ROMP-CCSD, respectively. In this scenario, the occupied-virtual block of the Fock matrix is not vanishing, and we treat it as a first-order perturbation. Note that since all calculations employ localized orbitals, the MP2 equations, as in Eq. (11), are of non-canonical type.

Among various choices for orbital localization, e.g., Pipek-Mezey [37], Foster-Boys [38], or selected column of the density matrix (SCDM) [39], we have opted for Atomic Valence Active Spaces (AVAS) [40]. Our choice is motivated by AVAS’s straightforward approach to defining valence occupied and virtual orbitals, along with its adaptability for incorporating higher angular momentum functions into the virtual space as discussed below. The objective of AVAS is to isolate a set of valence/semi-valence atomic orbitals ( $A$ ) denoted by  $p, q$ , which has overlap with the HF occupied ( $|i\rangle$ ) and virtual orbitals ( $|a\rangle$ ). To this end, we define the projection operator

$$P_A = \sum_{p,q \in A} [\sigma^{-1}]_{pq} |p\rangle \langle q|; \quad \sigma_{pq} = \langle p|q\rangle. \quad (16)$$

With this projection operator, we then construct two overlap matrices

$$[S^A]_{ij} = \langle i|P_A|j\rangle \quad \text{and} \quad [S^A]_{ab} = \langle a|P_A|b\rangle \quad (17)$$

in the space of occupied and virtual orbitals, respectively.

In order to isolate the active orbitals,  $[S^A]_{ij}$  and  $[S^A]_{ab}$  are diagonalized and the orbitals  $|i\rangle$  and  $|a\rangle$  are rotated by the diagonalizing matrices to generate two new sets of orbitals:  $|\tilde{i}\rangle$  and  $|\tilde{a}\rangle$ . We then choose the active orbitals to be the vectors in  $|\tilde{i}\rangle$  and  $|\tilde{a}\rangle$  corresponding to non-zero eigenvalues. In the construction of  $[S^A]_{ij}$  matrix, we can

freeze a few core molecular orbitals, which will then be added to the inactive set of orbitals.

Commonly, the minimal atomic orbital basis (MINAO) is employed for constructing  $A$ . However,  $A$  can also be constructed from a polarized set of atomic orbitals or intrinsic atomic orbitals (IAOs). In the latter case,  $P_A$  is constructed using

$$|p\rangle = \sum_{\mu} |\mu\rangle U_{\mu p}, \quad (18)$$

where  $[U_{\mu p}]$  is a submatrix of the IAO transformation matrix describing our choice of targeted atomic orbitals. Another important characteristic of the AVAS scheme is that instead of MINAO, one can use any small basis set allowing that the active space is spanned by orbitals of higher angular momentum. This particular aspect is important, for instance, in first-row transition metals, where often “double-shell” or 4d orbitals are required. However, this presents various possibilities to choose a small basis set that consists of a function of higher angular momentum. We will choose the minimal basis such that it exactly spans the set of A orbitals or active orbitals. This restriction is especially crucial for the occupied space. For the elements with higher atomic numbers, we will exclude a few core orbitals from the active space construction, and likewise a few core molecular orbitals can be frozen in the construction of  $[S^A]_{ij}$  overlap.

## IV. RESULTS

### A. Diatomic potential energy curves:

We apply the current method for a homo-diatomic molecule,  $N_2$ , and a hetero-diatomic molecule,  $CO$ , along a potential energy curve (PEC) to study the following aspects of the theory:

1. To assess the accuracy of different approaches, we analyze the PEC of these diatomic molecules with different approaches, namely MP2, both relaxed and unrelaxed versions of the MP-CCSD method and also the composite method. For the composite method, we modify Eq. (1) to make it a comparable uncoupled version of the current embedding scheme:

$$E_{\text{Composite}} = E_{\text{MP2,large}} + E_{\text{CC,small(fc)}} - E_{\text{MP2,small(fc)}}, \quad (19)$$

where large and small stand for large, small AO basis sets considered for the current calculation, and fc stands for the frozen core calculation.

We also compare the error in binding energy with respect to the CCSD method, using two metrics:

the Maximum Absolute Error (MAE) and the Non-Parallelity Error (NPE). We furthermore evaluate several spectroscopic parameters, namely, equilibrium bond distance ( $R_e$ ), harmonic frequency ( $\omega_e$ ), and first anharmonicity constant ( $\omega_e x_e$ ) by the least square fit of the PEC with a polynomial with high enough degree such that the parameter values converge.

2. We investigate the method’s convergence as we systematically increase the size of the active space aiming to demonstrate that this method is systematically improvable.
3. Additionally, we show the consistent behavior of the MP-CCSD method with increased AO basis set size, when we keep the active space fixed. This observation is significant, considering the challenges often encountered in achieving similar enhancements within many quantum embedding schemes, for example, with Schmidt decomposition-based DMET [41] and Bootstrap Embedding (BE)-DMET [42] methods.

For the active space in the current study, we choose the minimal valence active space along with the core, and subsequently add higher angular momentum shells, resulting in three different choices. In the following, we report those choices and the minimal basis (MINAO) used for IAO construction in each of the cases:

	active space	MINAO
A	1s 2s 2p	STO-3G
B	1s 2s 2p 3s 3p	SV
C	1s 2s 2p 3s 3p 3d	cc-pVDZ

Table I. Choices of active space for the diatomic molecules, and the small basis (denoted as MINAO) used for IAO construction.

#### 1. The nitrogen molecule ( $N_2$ ):

The PEC of  $N_2$  serves as a prototypical problem for many electronic structure methods due to the complexity involved in the dissociation of its triple bond. In this work, however, we will employ unrestricted single-reference electronic structure methods that can break the  $S^2$  symmetry of the electronic Hamiltonian. This symmetry breaking allows for the mixing of states of different spin-multiplicity, thus can simulate somewhat multi-reference behavior. Moreover, symmetry breaking in UHF also allows us to reach a lower-energy state variationally than the restricted method. The highest level method considered here, that is, unrestricted CCSD (UCCSD) is not very accurate quantitatively when we compared it against a higher rank CC method, UCCSDT. The MAE and NPE are 29 mH and 20 mH, respectively. But, it shows a correct dissociative behavior of the

ground state. UCCSD for the whole system will serve as a benchmark method.

We consider the aug-cc-pCVDZ and aug-cc-pCVTZ basis sets for the current study to analyze various aspects of the theory along with the basis set convergence.

In Fig. 2 we analyze the PEC obtained with various methods, where for the UMP-CCSD plots we consider B-type active space (see Table I) to show the general trend with embedded active space. We observe that the PECs obtained from various methods are not of similar quality, especially around the equilibrium region, where the Coulson-Fischer point is located, the UMP2 method and the composite methods show discontinuity. Both the relaxed and the unrelaxed versions of the UMP-CCSD remove that discontinuity. However, towards the dissociative limit, all the methods exhibit satisfactory behavior.

In Fig. 3 the differences between the tested methods relative to UCCSD are plotted. Here the binding energy was considered instead of the total energy. The figure shows that UMP2 differs significantly from UCCSD. This difference becomes maximal near the equilibrium region. Also close to the equilibrium, the UMP2 PEC shows a derivative discontinuity. The UMP-CCSD method reduces the MAE from 80 mH (UMP2) to 38 mH / 30 mH, and the NPE from 78 mH (UMP2) to 24 mH / 17 mH for A / B choice of active spaces, respectively. Similarly, the composite scheme reduces MAE and NPE to 24 mH and 24 mH, respectively. However, the difference curve both for the composite method and the UMP-CCSD appears not to be smooth around the equilibrium region, see Fig. 3. The energy difference curve corresponding to the composite method contains two derivative discontinuities which can be rationalized from the observation in Fig. 7 that it inherits two separate derivative discontinuities in the UMP2 method from two different basis sets. It also shows a possible weakness of the composite method along a PEC. The unrelaxed variant of UMP-CCSD shows a derivative discontinuity at the same bond distance as UMP2. This discontinuity can be lifted using the relaxed version of UMP-CCSD emphasizing the importance of orbital relaxation.

To improve the UMP-CCSD energies, we augment the active space with N 3d orbitals. To that end, we considered the cc-pVDZ basis set as our minimal basis in the AVAS scheme, which consists of one d-shell in the atomic basis. We report the relaxed and unrelaxed UMP-CCSD results in aug-cc-pCVDZ (DZ) and aug-cc-pCVTZ (TZ) basis set for active space choices B and C in Fig. 4. The plots in the left and right panels of Fig. 4 show that MAE and NPE have significantly improved compared to the smaller active space B. We emphasize that the error in binding energy is now well within the chemical accuracy ( $< 1$  kcal/mol) for the relaxed method and it is very close to the chemical accuracy ( $\approx 2$  kcal/mol) with the unrelaxed method.

We will now analyze the AO basis set convergence with the plot in Fig. 4. In this context, we have considered B- and C- type active spaces and then enlarged the basis set

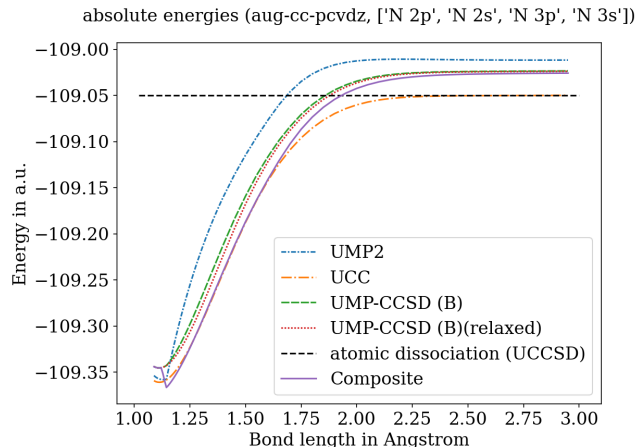


Figure 2. PEC of  $N_2$  molecule in aug-cc-pCVDZ basis set with various methods. B active space is as described in Table I

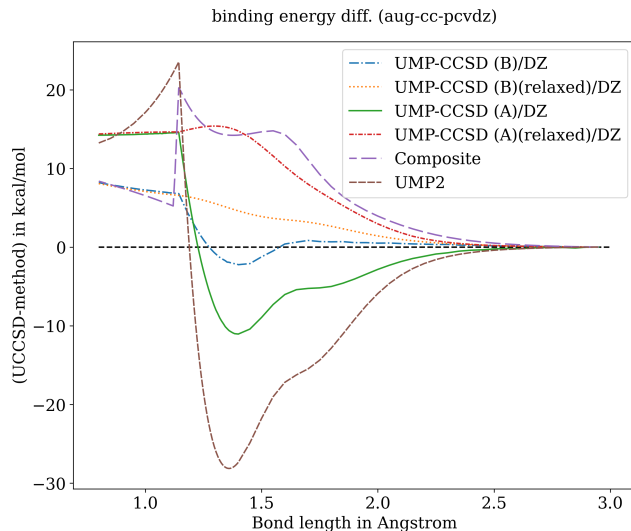


Figure 3. Binding energy error with respect to UCCSD along a PEC for  $N_2$  in aug-cc-pCVDZ basis set. A and B active spaces are as described in Table I. DZ stands for the aug-cc-pCVDZ basis set.

from aug-cc-pCVDZ to aug-cc-pCVTZ for each of them. We will study the error between the embedding scheme and UCCSD as we increase the basis set size. For relaxed UMP-CCSD, we observe a nearly constant error as we increase the AO basis from double- $\zeta$  to triple- $\zeta$  quality. However, for the unrelaxed UMP-CCSD variant, we observe that the difference from a small basis set to a large basis set is substantial. Thus, we conclude that we do not lose accuracy when enlarging the basis set with the relaxed version of the embedding scheme.

The quality of the PEC and the difference curve with various methods, as described so far, influences the spectroscopic parameters as shown in Table II. Compared to UCCSD, we observe that UMP-CCSD reproduces  $R_e$ ,  $\omega_e$  and  $\omega_e x_e$  better than the composite method and UMP2.

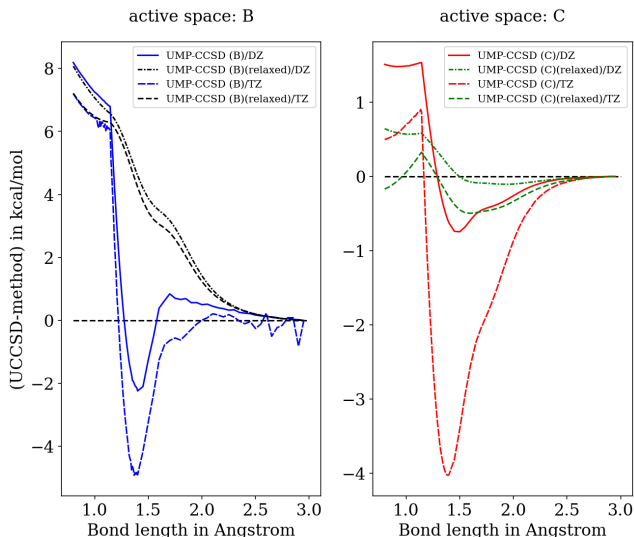


Figure 4.  $N_2$  binding energy error with respect to UCCSD in aug-cc-pCVDZ (denoted as DZ) and aug-cc-pCVTZ (denoted as TZ) basis sets. B and C active spaces are as described in Table I.

Method	$\Delta R_e$ (in Å)	$\Delta \omega_e$ (in $\text{cm}^{-1}$ )	$\Delta \omega_e x_e$ (in $\text{cm}^{-1}$ )
UMP2	0.0059	1230.06	120.3261
Composite	0.0539	327.78	320.5781
UMP-CCSD (C)	0.0003	86.85	-6.8039
UMP-CCSD (C)(relaxed)	0.0006	2.60	-1.7131

Table II. Spectroscopic parameters of  $N_2$  evaluated in aug-cc-pCVTZ basis set. We reported the difference w.r.t. the UCCSD method for all the spectroscopic parameters. In UMP-CCSD (C), C stands for the active space defined in Table I.

The failure of the composite method and UMP2 in estimating  $\omega_e$  and  $\omega_e x_e$  can be attributed to the discontinuities in the PEC near the equilibrium region.

Although the relaxed and unrelaxed variants of UMP-CCSD yield similar MAE and NPE along the PEC, the energy difference plots around the equilibrium region become much smoother when orbital relaxations are considered. This improvement is reflected in the spectroscopic parameters  $\omega_e$  and  $\omega_e x_e$ , which are coefficients to the higher order terms in the polynomial. They now become significantly closer to the corresponding UCCSD results when orbital relaxations are taken into account. Hence, the self-consistency cycle improves the behavior around the equilibrium region significantly.

## 2. Carbon monoxide (CO):

We now consider a hetero-diatom molecule – carbon monoxide – following a similar testing structure as in the preceding  $N_2$  example. We begin our investigations

by comparing corresponding PEC for UMP2, UCCSD, relaxed and unrelaxed UMP-CCSD, and the composite method, see Fig. 9. We observe that the PEC corresponding to UMP2 exhibits two discontinuities near the equilibrium region. The composite method improves the behavior around the equilibrium region, however, it deteriorates away from the equilibrium region. In comparison, both the relaxed and unrelaxed versions of UMP-CCSD remove the discontinuities in the PEC.

Computing the binding energy difference curves in Fig. 5 (top panel) shows two derivative discontinuities in the UMP2 curve and multiple derivative discontinuities in the composite method’s curve. The latter can be attributed to the composite method inheriting discontinuities from the individual computations; for the CO molecule, we see that multiple discontinuities appear at different bond distances for different basis sets, see “UMP2 (large)” and “UMP2 (small)” graphs in Fig. 8. Using the unrelaxed version of UMP-CCSD, we observe one derivative discontinuity, which can be lifted by including orbital relaxations.

We also calculate the spectroscopic parameters  $R_e$ ,  $\omega_e$  and  $\omega_e x_e$  for the carbon monoxide molecule, which are listed in Table III. Compared to the preceding  $N_2$  example, we note that the composite method shows noticeable improvement over UMP2 for all computed quantities. We attribute this to the qualitative agreement of the composite method’s PEC with the PEC of UCCSD near the equilibrium region, see Fig. 9, as well as the fact that the discontinuities appear further away from the equilibrium. We still observe that  $R_e$  and  $\omega_e$  are best reproduced with the UMP-CCSD method, showing a consistent improvement over the composite method.

In the bottom panel of Fig. 5, we plot the error in the binding energy of UMP-CCSD and the composite method relative to UCCSD. Similar to our observations in the  $N_2$  example, we find that for the carbon monoxide molecule, we do not lose accuracy when enlarging the basis set from aug-cc-pCVDZ and aug-cc-pCVTZ. The error curves for both basis sets agree satisfactorily with each other (within 1 kcal/mol). Additionally, we have compared the relative accuracy of the composite scheme, i.e. the uncoupled version of the embedding scheme, on the same plot. For this scheme, the extent of agreement varies across the potential energy curve (PEC), and it is quantitatively worse than the UMP-CCSD method.

## B. W4 Dataset:

We now investigate the accuracy of the current method on thermochemical energy differences using the well-known W4-11 [43] dataset. This dataset consists of various chemical reactions of a total of 152 molecules and atoms from the 1st, 2nd and 3rd row of the periodic table. Most of the species in this dataset can be characterized as single reference (SR) systems, except for a small number of multi-reference (MR) characters. We

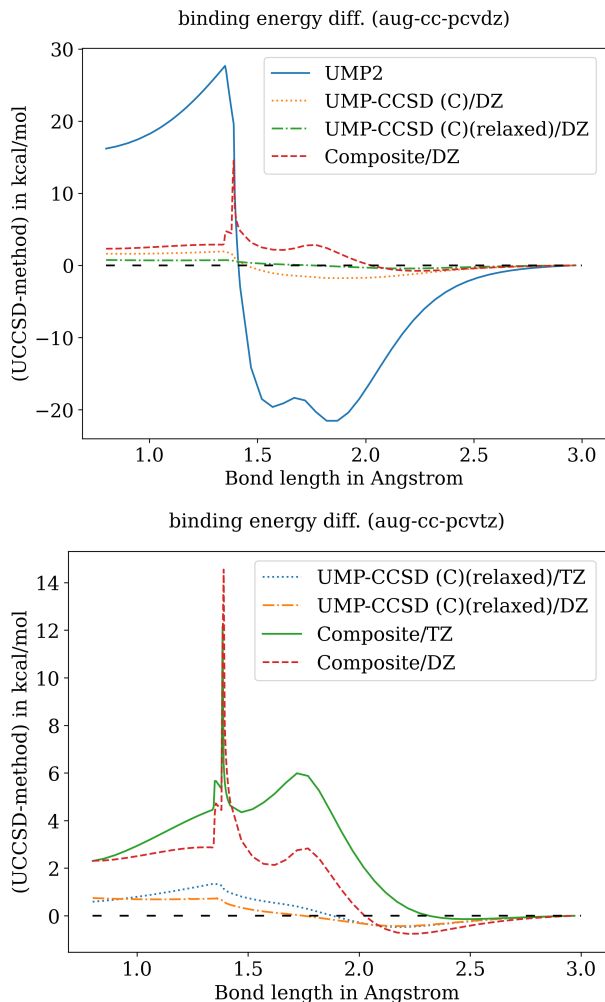


Figure 5. Binding energy differences w.r.t. UCCSD along a PEC for CO. DZ and TZ are abbreviations for aug-cc-pCVDZ and aug-cc-pCVTZ basis sets respectively.

Method	$\Delta R_e$ (in Å)	$\Delta\omega_e$ (in $\text{cm}^{-1}$ )	$\Delta\omega_e x_e$ (in $\text{cm}^{-1}$ )
UMP2	0.0101	-105.82	1.221
Composite	0.0017	-12.76	-0.0878
UMP-CCSD (C)	0.0007	-6.73	-0.1200
UMP-CCSD (C)(relaxed)	0.0005	-4.65	0.0817

Table III. Spectroscopic parameters of CO evaluated in aug-cc-pCVTZ basis set. We reported the difference to the UCCSD results for all spectroscopic parameters. Note that “(C)” in “UMP-CCSD (C)”, stands for the active choice defined in Table I.

compute all the SR systems in this dataset, for which UCCSD serves as the benchmark results. The MR systems are less accurately described than the SR systems when treated with UCCSD [44], we therefore do not include them in our comparison. In total, we compute 140 atomization energies (TAE) and bond dissociation ener-

gies (BDE), 20 isomerization energies (ISO), 505 heavy atom transfer (HAT), and 13 nucleophilic substitution (SN) reactions. We note that the benchmarks for the SR problems in this dataset can be computed to chemical accuracy using CCSD(T) or even beyond. However, we here employ the dataset to investigate the accuracy of (relaxed) UMP-CCSD relative to UCCSD in the cc-pCVTZ basis set. To that end, we compare UMP2, the composite method and relaxed UMP-CCSD to UCCSD. For the choice of active space, valence occupied and valence virtual orbitals are augmented with an additional atomic orbital shell to expand the active virtual orbital space. This implies that for the elements in the second row 2s, 2p, 3s, 3p and 3d orbitals are considered within the active space, and for the elements in the third row 2s, 2p, 3s, 3p, 3d, 4s, 4p orbitals are considered. To achieve this goal, we have chosen cc-pVDZ as the small basis reference for IAO construction for all the atoms.

Figure 6 shows violin plots of the absolute errors relative to UCCSD for different thermochemical reactions. We observe that the mean absolute error (MAE) in UMP-CCSD has significantly improved compared to UMP2 for all tested reactions. Moreover, we observe that UMP-CCSD, on average, provides a significant improvement over the results computed with the composite method. We emphasize that the MAE of UMP-CCSD is within chemical accuracy for all the reactions considered in this study. Additionally, we observe that the maximal spread of the deviation is also much more favorable for UMP-CCSD in comparison to the other methods considered.

## V. CONCLUSION:

We have proposed and numerically scrutinized a new quantum embedding scheme – named MP-CC – where the local/fragment problem is solved with the coupled cluster (CC) level, and the environment problem is solved at a level similar to the Møller–Plesset (MP) perturbation theory. Instead of constructing a density matrix or Green’s function at the CC level, the proposed embedding scheme relies only on the cluster amplitudes to separate the environment and the fragment problem. The self-consistency in the whole procedure is ensured by defining a set of amplitude equations coupling the fragment and the environment. In particular, we do not need to construct a hybridization term between these two layers to take “environment fluctuations” into account. Instead, a class of amplitudes,  $T^M$  that couples those two layers is self-consistently solved. Furthermore, the interaction term for the fragment problem is renormalized by the amplitudes from a low-level method describing the environment problem.

This work provides a general framework allowing the use of different low-level methods for computing the environment problem, while the high-level method for the fragment problem remains fixed as a CC method. In this work, we have proposed and compared two different

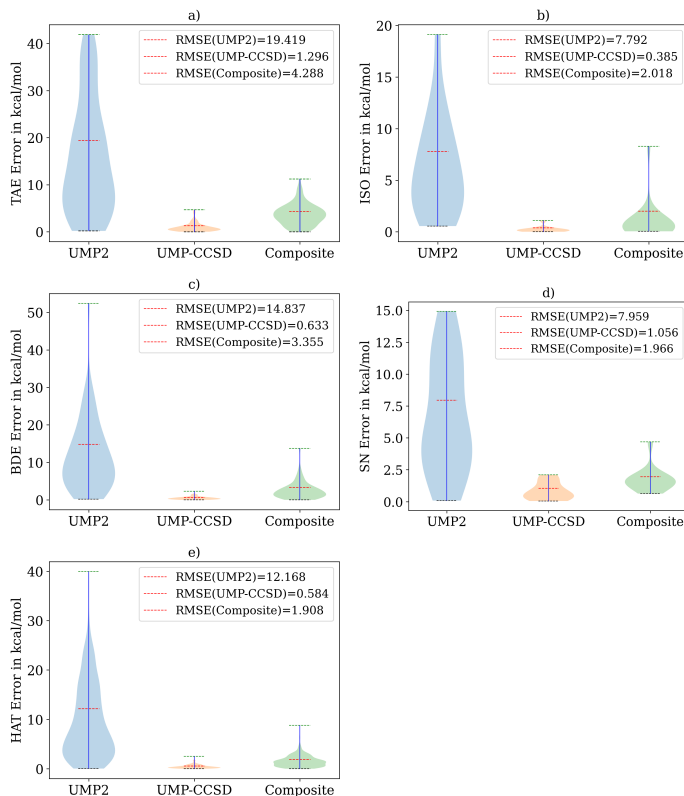


Figure 6. Violin plot of the errors of UMP2, UMP-CCSD, and composite method compared to the corresponding CCSD results for various thermochemical reactions with W4-11 dataset in cc-pCVTZ basis set. The different panels show a) the total atomization energy, b) the isomerization energy, c) the bond dissociation energy, d) the nucleophilic substitution reaction energy, and e) the heavy atom transfer energy.

heuristics for the low-level method: one without orbital relaxation and one with orbital relaxation. We have observed that the unrelaxed version of the low-level method noticeably improves upon the UMP2 method as well as the composite method by removing discontinuities in diatomic PECs of the  $N_2$  and CO molecules. The relaxed version of the low-level method further improves upon the unrelaxed one by removing a derivative discontinuity in the error curve relative to UCCSD results, thus making it qualitatively similar to the CCSD method. Although the composite method (or the uncoupled version of the embedding method considered in this work) numerically improves upon the UMP2 method, it inherits qualitative failures of the UMP2 method. In particular, it shows discontinuities in the symmetry-breaking regions, making it unreliable over a PEC. A significant finding of our work is

that we achieve similar accuracy for a fixed active space size when the basis set size is increased, which can generally not be guaranteed for embedding methods. This observation holds for the relaxed version of our method where we allow coupling between the system and the environment layers.

We have moreover investigated the reliability of the proposed orbital relaxed UMP-CCSD method for single reference systems in the W4-11 thermochemistry dataset. Our investigations show that UMP-CCSD reproduces, on average, the UCCSD results for the single reference systems in the W4-11 thermochemistry dataset to chemical accuracy.

For future works, it will be interesting to investigate other heuristics for the low-level method, e.g., Brillouin-Wigner perturbation theory (BWPT) [45], random phase approximation (RPA) or ring coupled cluster doubles (r-CCD). A preliminary analysis has shown that the current method has a favorable scaling when including triples amplitudes; we will investigate if UMP-CCSDT also reproduces UCCSDT results with similar accuracy, as reported in this UMP-CCSD study. For the current formulation, there is an unfavorable scaling ( $\mathcal{O}(n_v^2 n_o^2 n_{o,act} n_{v,act})$ ) when the renormalized interaction is built before solving the fragment amplitude equations (see Fig. 1). In the future, we plan to explore approximation schemes to construct the renormalized interaction, such that we can achieve even lower polynomial scaling for the full scheme. Such construction will also facilitate working out an efficient multi-fragment approach, which is commonly employed by embedding approaches such as LASSCF [46–49], DMET [41, 50–53], SEET [54, 55], DMFT [56–58] or g-RISB [59, 60]. Moreover, we have not utilized any efficient local correlation ideas to reduce the complexity further—this is another objective for future works.

## VI. ACKNOWLEDGEMENTS

This material is based upon work supported by the U.S. Department of Energy, Office of Science, Office of Advanced Scientific Computing Research and Office of Basic Energy Sciences, Scientific Discovery through Advanced Computing (SciDAC) program under Award Number DE-SC0022198 (A.S., K.B.W. and L.L.), and Award Number DE-SC0022364 (M.H-G.) and by the Simons Targeted Grants in Mathematics and Physical Sciences on Moiré Materials Magic (F.F.). L.L. is a Simons Investigator in Mathematics. A.S. and L.L. thank Karol Kowalski for insightful discussions.

[1] S. Saebo and P. Pulay, *Annu. Rev. Phys. Chem.* **44**, 213 (1993).

[2] C. Riplinger and F. Neese, *J. Chem. Phys.* **138**, 034106 (2013).

- [3] Q. Ma and H.-J. Werner, *WIREs Comput Mol. Sci.* **8**, e1371 (2018).
- [4] J. E. Subotnik, A. Sodt, and M. Head-Gordon, *J. Chem. Phys.* **125**, 074116 (2006).
- [5] G. Knizia, T. B. Adler, and H.-J. Werner, *J. Chem. Phys.* **130**, 054104 (2009).
- [6] A. Irmeler and A. Grüneis, *J. Chem. Phys.* **151**, 104107 (2019).
- [7] T. Helgaker, W. Klopper, H. Koch, and J. Noga, *J. Chem. Phys.* **106**, 9639 (1997).
- [8] M. Caffarel and W. Krauth, *Phys. Rev. Lett.* **72**, 1545 (1994).
- [9] E. Gull, A. J. Millis, A. I. Lichtenstein, A. N. Rubtsov, M. Troyer, and P. Werner, *Rev. Mod. Phys.* **83**, 349 (2011).
- [10] F. A. Wolf, A. Go, I. P. McCulloch, A. J. Millis, and U. Schollwöck, *Phys. Rev. X* **5**, 041032 (2015).
- [11] H.-J. Werner, G. Knizia, C. Krause, M. Schilwilk, and M. Dornbach, *J. Chem. Theory Comput.* **11**, 484 (2015).
- [12] P. Pinski, C. Riplinger, E. F. Valeev, and F. Neese, *J. Chem. Phys.* **143**, 034108 (2015).
- [13] Z. Wang, A. Aldossary, and M. Head-Gordon, *J. Chem. Phys.* **158**, 064105 (2023).
- [14] N. P. Bauman, E. J. Bylaska, S. Krishnamoorthy, G. H. Low, N. Wiebe, C. E. Granade, M. Roetteler, M. Troyer, and K. Kowalski, *J. Chem. Phys.* **151**, 014107 (2019).
- [15] K. Kowalski, *J. Chem. Phys.* **158**, 054101 (2023).
- [16] R. H. Myhre, A. M. J. Sánchez de Merás, and H. Koch, *J. Chem. Phys.* **141**, 224105 (2014).
- [17] S. D. Folkestad, E. F. Kjørstad, L. Goletto, and H. Koch, *J. Chem. Theory Comput.* **17**, 714 (2021).
- [18] J. A. Pople, M. Head-Gordon, D. J. Fox, K. Raghavachari, and L. A. Curtiss, *J. Chem. Phys.* **90**, 5622 (1989).
- [19] L. A. Curtiss, K. Raghavachari, G. W. Trucks, and J. A. Pople, *J. Chem. Phys.* **94**, 7221 (1991).
- [20] L. A. Curtiss, K. Raghavachari, P. C. Redfern, V. Rassolov, and J. A. Pople, *J. Chem. Phys.* **109**, 7764 (1998).
- [21] L. A. Curtiss, P. C. Redfern, and K. Raghavachari, *J. Chem. Phys.* **126**, 084108 (2007).
- [22] J. M. L. Martin and G. de Oliveira, *J. Chem. Phys.* **111**, 1843 (1999).
- [23] A. D. Boese, M. Oren, O. Atasoylu, J. M. L. Martin, M. Kállay, and J. Gauss, *J. Chem. Phys.* **120**, 4129 (2004).
- [24] A. Karton, E. Rabinovich, J. M. L. Martin, and B. Ruscic, *J. Chem. Phys.* **125**, 144108 (2006).
- [25] A. Tajti, P. G. Szalay, A. G. Császár, M. Kállay, J. Gauss, E. F. Valeev, B. A. Flowers, J. Vázquez, and J. F. Stanton, *J. Chem. Phys.* **121**, 11599 (2004).
- [26] T. Helgaker, P. Jørgensen, and J. Olsen, *Molecular electronic-structure theory* (John Wiley & Sons, 2013).
- [27] G. Knizia, *J. Chem. Theory Comput.* **9**, 4834 (2013).
- [28] N. C. Handy and I. Schaefer, Henry F., *J. Chem. Phys.* **81**, 5031 (1984).
- [29] H. Koch, H. J. A. Jensen, P. Jørgensen, T. Helgaker, G. E. Scuseria, and I. Schaefer, Henry F., *J. Chem. Phys.* **92**, 4924 (1990).
- [30] D. J. Thouless, *Nuclear Physics* **21**, 225 (1960).
- [31] O. Christiansen, H. Koch, and P. Jørgensen, *Chemical Physics Letters* **243**, 409 (1995).
- [32] E. G. C. P. van Loon, M. Rösner, M. I. Katsnelson, and T. O. Wehling, *Phys. Rev. B* **104**, 045134 (2021).
- [33] X.-J. Han, P. Werner, and C. Honerkamp, *Phys. Rev. B* **103**, 125130 (2021).
- [34] Q. Sun, X. Zhang, S. Banerjee, P. Bao, M. Barbry, N. S. Blunt, N. A. Bogdanov, G. H. Booth, J. Chen, Z.-H. Cui, J. J. Eriksen, Y. Gao, S. Guo, J. Hermann, M. R. Hermes, K. Koh, P. Koval, S. Lehtola, Z. Li, J. Liu, N. Mardirossian, J. D. McClain, M. Motta, B. Mussard, H. Q. Pham, A. Pulkin, W. Purwanto, P. J. Robinson, E. Ronca, E. R. Sayfutyarova, M. Scheurer, H. F. Schurkus, J. E. T. Smith, C. Sun, S.-N. Sun, S. Upadhyay, L. K. Wagner, X. Wang, A. White, J. D. Whitfield, M. J. Williamson, S. Wouters, J. Yang, J. M. Yu, T. Zhu, T. C. Berkelbach, S. Sharma, A. Y. Sokolov, and G. K.-L. Chan, *J. Chem. Phys.* **153**, 024109 (2020).
- [35] Q. Sun, T. C. Berkelbach, N. S. Blunt, G. H. Booth, S. Guo, Z. Li, J. Liu, J. D. McClain, E. R. Sayfutyarova, S. Sharma, *et al.*, Wiley Interdisciplinary Reviews: Computational Molecular Science **8**, e1340 (2018).
- [36] Q. Sun, *Journal of computational chemistry* **36**, 1664 (2015).
- [37] J. Pipek and P. G. Mezey, *J. Chem. Phys.* **90**, 4916 (1989).
- [38] S. F. Boys, *Rev. Mod. Phys.* **32**, 296 (1960).
- [39] A. Damle, L. Lin, and L. Ying, *J. Chem. Theory Comput.* **11**, 1463 (2015).
- [40] E. R. Sayfutyarova, Q. Sun, G. K.-L. Chan, and G. Knizia, *J. Chem. Theory Comput.* **13**, 4063 (2017).
- [41] G. Knizia and G. K.-L. Chan, *J. Chem. Theory Comput.* **9**, 1428 (2013).
- [42] H.-Z. Ye and T. Van Voorhis, *J. Phys. Chem. Lett.* **10**, 6368 (2019).
- [43] A. Karton, S. Daon, and J. M. Martin, *Chem. Phys. Lett.* **510**, 165 (2011).
- [44] J. Lee, H. Q. Pham, and D. R. Reichman, *J. Chem. Theory Comput.* **18**, 7024 (2022), PMID: 36255074.
- [45] K. Carter-Fenk and M. Head-Gordon, *J. Chem. Phys.* **158**, 234108 (2023).
- [46] M. R. Hermes and L. Gagliardi, *J. Chem. Theory Comput.* **15**, 972 (2019).
- [47] M. R. Hermes, R. Pandharkar, and L. Gagliardi, *J. Chem. Theory Comput.* **16**, 4923 (2020).
- [48] H. Q. Pham, V. Bernales, and L. Gagliardi, *J. Chem. Theory Comput.* **14**, 1960 (2018).
- [49] V. Agarawal, D. King, M. Hermes, and L. Gagliardi, *ChemRxiv* (2024), 10.26434/chemrxiv-2024-sbp4r.
- [50] G. Knizia and G. K.-L. Chan, *Phys. Rev. Lett.* **109**, 186404 (2012).
- [51] H. Q. Pham, V. Bernales, and L. Gagliardi, *J. Chem. Theory Comput.* **14**, 1960 (2018).
- [52] M. Nusspickel and G. H. Booth, *Phys. Rev. X* **12**, 011046 (2022).
- [53] M. Nusspickel, B. Ibrahim, and G. H. Booth, *J. Chem. Theory Comput.* **19**, 2769 (2023).
- [54] A. A. Kananenka, E. Gull, and D. Zgid, *Phys. Rev. B* **91**, 121111(R) (2015).
- [55] S. Isakov, C.-N. Yeh, E. Gull, and D. Zgid, *Phys. Rev. B* **102**, 085105 (2020).
- [56] A. Georges, G. Kotliar, W. Krauth, and M. J. Rozenberg, *Rev. Mod. Phys.* **68**, 13 (1996).
- [57] G. Kotliar, S. Y. Savrasov, K. Haule, V. S. Oudovenko, O. Parcollet, and C. A. Marianetti, *Rev. Mod. Phys.* **78**, 865 (2006).
- [58] V. I. Anisimov, A. I. Poteryaev, M. A. Korotin, A. O. Anokhin, and G. Kotliar, *J. Phys.: Condensed Matter*

9, 7359 (1997).  
 [59] T.-H. Lee, T. Ayrál, Y.-X. Yao, N. Lanata, and G. Kotliar, *Phys. Rev. B* **99**, 115129 (2019).

[60] T.-H. Lee, N. Lanatà, and G. Kotliar, *Phys. Rev. B* **107**, L121104 (2023).

---

### Appendix A: Comparison with the MLCC method

In the multi-level CC (MLCC) method, Koch and co-workers defined a wave function ansatz

$$|\Psi\rangle = e^X |\Phi_0\rangle; \quad X = T_1 + T_2^{act} + T_2^{inact} \quad (\text{A1})$$

where,  $T_1$  is both an active and inactive set of singles amplitudes,  $T_2^{act}$ , and  $T_2^{inact}$  stand for active, and inactive doubles amplitudes. Then to derive the inactive projection equations as in Eq. (8), they assign a perturbative order for  $T_2^{inact}$ , but the rest are treated in all orders. Furthermore, the projection equation for inactive  $T_1$  amplitudes is the same as CC amplitude equations, but the one for  $T_2^{inact}$  is truncated at the first order. The projection equations for  $T_2$  active amplitudes do not differ from CC. This scheme is similar to using CC2 [31] equations for the inactive amplitudes. Then, to include triples excitation, they augment  $X$  with active triples amplitudes,  $T_3^{act}$ . Therefore, their treatment of the doubles and triples amplitudes are not on the same footing. With this ansatz their low-level projection equations contain singles and doubles equations, but no triples equations. When triples are included in that work, both for the singles and doubles equations, there is a  $[V, T_3]$  term. But because of the active restriction in  $T_3$ , it maximally scales as  $n_{v,act}^3 n_{o,act}^3 n_v$ .

Our projection equations for the active amplitudes are full CC amplitude equations similar to the MLCC method, but the inactive projection equations are derived differently than that method. We don't define a wave function ansatz for the total problem but tried to pick a subset of terms/diagrams from the full set of terms of the CC amplitude equation. This subset of terms is chosen based on a certain heuristic that ensures the low-scaling nature of the inactive amplitude equation. It allows us to choose a projection equation like Eqs. (12) and (13), where we have truncated both the singles and doubles equations at the same order of perturbation, unlike the CC2 projection equations. This choice produces a minimal model that can induce orbital relaxation for the environment when the active space/fragment  $T_1$  amplitudes become nonzero. When we include active  $T_3$  equations for the fragment, it does not give rise to any new sets of inactive  $T_3$  amplitudes because of the lack of  $[V, T_3]$  or  $[V, T_2]$  terms which are second-order terms (note that, the perturbative order argument here is different than the Møller-Plesset perturbation series as we treat  $T_1$  amplitudes to all order for the low-level method). Therefore, with our approach when triples are included, the complexity of the low-level equations doesn't increase compared to the singles-doubles equations.

### Appendix B: Additional plots

We have added Fig. 7 and 8 to aid the analysis of composite method over the PEC of  $N_2$  and CO respectively. Additionally, Fig. 9 was added to show the section of PEC of CO where multiple discontinuities arise for the UMP2 method and the composite method.

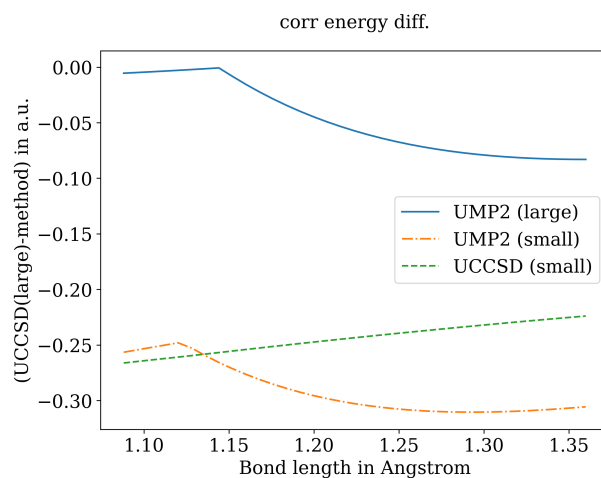


Figure 7. Correlation energy differences w.r.t. UCCSD in aug-cc-pCVDZ basis set along a PEC for N<sub>2</sub>. large and small basis sets stand for aug-cc-pCVDZ and SVP respectively.

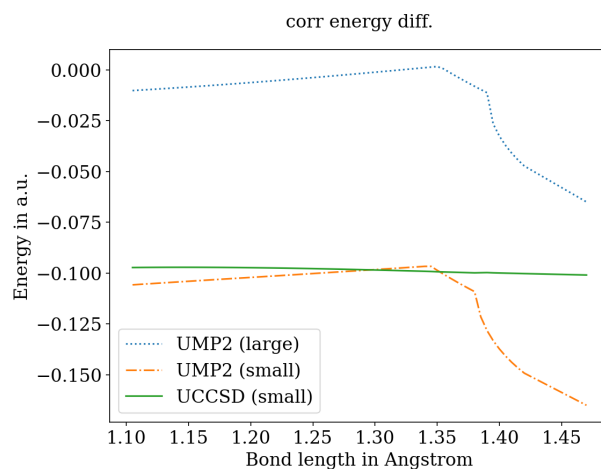


Figure 8. Correlation energy differences w.r.t. UCCSD in aug-cc-pVDZ basis set along a PEC for CO. large and small basis sets stand for aug-cc-pCVDZ and cc-pVDZ respectively.

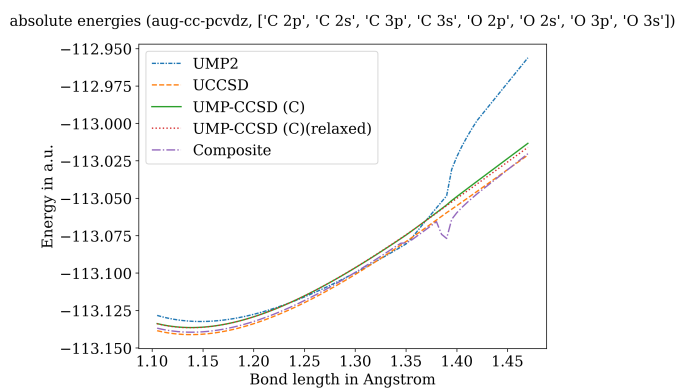


Figure 9. Correlation energy differences w.r.t. UCCSD in aug-cc-pCVDZ basis set along a PEC for CO. large and small basis sets stand for aug-cc-pVDZ and DZ respectively.